Appl Water Sci (2017) 7:2287–2295
DOI 10.1007/s13201-016-0404-5

ORIGINAL ARTICLE

# Competitive sorption of $Cd^{2+}$ and $Pb^{2+}$ from a binary aqueous solution by poly (methyl methacrylate)-grafted montmorillonite clay nanocomposite

**Tavengwa Bunhu[1] · Lilian Tichagwa[1] · Nhamo Chaukura[2]**

Received: 24 November 2015 / Accepted: 14 March 2016 / Published online: 24 March 2016


**Abstract** Poly(methyl methacrylate)-grafted montmorillonite (PMMAgMMT) clay and sodium-exchanged montmorillonite (NaMMT) clay were prepared through in situ graft polymerisation and used to remove $Cd^{2+}$ and $Pb^{2+}$ from synthetic wastewater. The modification of adsorbent materials was confirmed by fourier transform infra-red spectroscopy (FTIR), thermogravimetric analysis (TGA) and X-ray powder diffraction (XRD) techniques. BET surface area measurements showed NaMMT had a higher surface area than PMMAgMMT. Batch experiments were used to assess the simultaneous uptake of $Cd^{2+}$ and $Pb^{2+}$ from a synthetic binary solution. $Pb^{2+}$ was preferentially sorbed, exhibiting greater affinity for the sorbents compared to $Cd^{2+}$ as shown by its relatively higher uptake onto the sorbents than $Cd^{2+}$. The maximum sorption capacities for NaMMT and PMMAgMMT were 18.73 and 19.27 mg/g for $Cd^{2+}$, and 30.03 and 34.25 mg/g for $Pb^{2+}$, respectively. The sorption data obeyed the Langmuir model and the pseudo-second order kinetic model with $R^2$ of at least 0.9800 for both models. The sorbents could also be regenerated up to three cycles without a significant loss in the sorption capacity. FTIR measurements showed the presence of metal–oxygen bonds after sorption, confirming the occurrence of adsorption as one of the heavy metal removal processes. The work demonstrated the potential of using low-cost nanoscale composite material for the removal of $Cd^{2+}$ and $Pb^{2+}$ from aqueous solution.

**Keywords** Competitive sorption · Cadmium · Lead · PMMA-grafted montmorillonite

## Introduction

The supply of clean water to communities is of paramount importance, and is a challenge, especially in developing countries. Heavy metals such as cadmium and lead are some of the most toxic inorganic contaminants found in water bodies (Jin et al. 2004; Tran et al. 2015). Exposure to these metals has been associated with many health effects including renal damage (Jarup et al. 2000; Nawrot et al. 2010), osteoporosis and bone defects (Alfven et al. 2002; Kazantzis 2004). These two heavy metals are released into the aquatic systems from a number of industrial processes such as metal plating, smelting, mining, cadmium–nickel and lead batteries, phosphate fertilizers, paint industries, leather tanning, pigments, textiles and alloy industries as well as from sewage (Kobya et al. 2005; Teemu 2007).

Many conventional methods for the removal of heavy metals from contaminated water such as precipitation, flocculation, solvent extraction, ion exchange, reverse osmosis and membrane filtration are limited by poor removal efficiencies and high cost (Pavasant et al. 2006; Arief et al. 2008). Sorption onto a solid matrix has become one of the preferred methods for the removal of toxic contaminants from water. This method is reported to be effective, economical, versatile and relatively simple (Garg et al. 2004). Nanoclays, especially smectites, have been widely used as adsorbents due to their high specific surface area, high chemical and mechanical stability as well as

✉ Nhamo Chaukura
nchaukura@gmail.com

[1] Department of Pure and Applied Chemistry, University of Fort Hare, P. Bag X1314, Alice Campus, Alice 5700, South Africa

[2] Department of Polymer Technology and Engineering, Harare Institute of Technology, PO Box BE 277, Belvedere, Harare, Zimbabwe

their ion exchange capabilities (Cao et al. 2009; Zhu et al. 2016a, b). Previous studies have reported enhanced removal capacities by pristine montmorillonite clay or after various treatments, e.g., acid washing, thermal treatment, or surfactant modification for the removal of specific pollutants (Fan et al. 2014; Zhu et al. 2016a, b). The use of poly(methyl methacrylate)-grafted montmorillonite in competitive sorption of heavy metals like $Cd^{2+}$ and $Pb^{2+}$ has not been reported elsewhere. The advantages of this sorbent include excellent sorption properties, ease of availability of montmorillonite, environmental friendliness, and its associated low cost (Qin et al. 2015; Tran et al. 2015; Xing et al. 2015; Zhu et al. 2016a, b). Generally, wastewater contains a variety of pollutants and the presence of one pollutant will affect the uptake or removal of other pollutants through sorption. Waste waters from different sources may also contain more than one metal ion, it is usually a mixture of a number of metal ions often together with organic dyes or solvents in varying concentrations. The aim of this study was therefore, to assess the simultaneous adsorption of $Cd^{2+}$ and $Pb^{2+}$ from aqueous solution onto polymer-grafted montmorillonite clay, and its effect on the adsorption isotherms and kinetics.

For a given mass of adsorbent, $m$ in a solution volume, $V$ and initial concentration $C_0$, the amount of metal ions adsorbed, $Q$ at time, $t$ is computable using Eq. 1 (Gwenzi et al. 2014):

$$Q_t = \frac{V(C_0 - C_t)}{m} \tag{1}$$

$C_t$ is the concentration in solution at time $t$.

Adsorption isotherms provide information on the sorption of an adsorbate for a given adsorbent and predict distribution of the adsorbate between the surface and solution (Rebitanim et al. 2012). When an adsorbent is in contact with the surrounding fluid of a certain concentration, adsorption occurs and after a while the adsorbent and the fluid reach equilibrium. The commonly used adsorption isotherm models are the Langmuir and the Freundlich models (Cabrera et al. 2014). For an equilibrium amount of adsorbate, $C_e$ and equilibrium sorption capacity of adsorbent, $Q_e$, the Langmuir model (Eq. 2) is used for the estimation of maximum adsorption capacity of the adsorbent:

$$\frac{C_e}{Q_e} = \frac{1}{Q_0 b} = \frac{C_e}{Q_0} \tag{2}$$

where $Q_0$ and $b$ are the Langmuir constants related to the adsorption capacity and the rate of adsorption, respectively.

The model assumes that absorption sites have equal affinities for molecules of the adsorbate and adsorption at one site does not affect the ability of the next site to adsorb heavy metal ions (Kumar et al. 2008; Wang et al. 2009; Rebitanim et al. 2012). Furthermore each site can accommodate only one molecule or ion and adsorption at the surface is localized, adsorbed molecules or ions are adsorbed at specific sites.

The Freundlich model (Eq. 3) describes the adsorption equilibrium at heterogeneous surfaces and does not assume monolayer capacity:

$$\mathrm{Log}Q_e = \mathrm{Log}K_f + \frac{1}{n}\mathrm{Log}C_e \tag{3}$$

where $K_f$ and $n$ are the Freundlich constants related to the adsorption capacity and the rate of adsorption, respectively.

Adsorption kinetics can be described using Lagergren linear first-order and second-order kinetics as described by Eqs. 4 and 5, respectively (Delval et al. 2002; Ruziwa et al. 2015). For an amount of solute adsorbed at equilibrium per unit mass of adsorbent, $Q_e$, and amount of solute adsorbed $Q_t$ at time $t$, the Lagergren linear pseudo first-order equation is shown in Eq. 4:

$$\mathrm{Log}(Q_e - Q_t) = \mathrm{Log}Q_e - \frac{k_1}{2.303}t \tag{4}$$

where $k_1$ is the pseudo first-order rate constant.

The pseudo second-order equation is:

$$\frac{t}{Q_t} = \frac{t}{k_2 Q_e^2} + \frac{t}{Q_e} \tag{5}$$

where $k_2$ is the pseudo second-order rate constant.

The pseudo second-order model assumes chemisorption and can be used to describe the adsorption mechanism for the whole sorption process.

## Experimental

### Materials

Dodecylbenzene sulphonic acid (DBS) and sodium metabisulphite (SMBS) from BDH Chemicals; ammonium persulphate (AMPS, 98 %) from Associated Chemical Enterprises, acetone (99 %) from SMM Chemicals and tetrahydrofuran (99.5 %) from Fluka were used without any purification or pretreatment. $Pb(NO_3)_2$ (99.5 %), methyl methacrylate (MMA, 99 %) were purchased from SAARCHEM (Pty) Ltd. MMA was first distilled before use and $Pb(NO_3)_2$ and $Cd(NO_3)_2{\cdot}4H_2O$ were used as received. Montmorillonite (MMT) (cation exchange capacity (CEC): 91.44 meq/100 g) from BaoBio Holdings (Pty) Ltd was used as supplied.

### Graft polymerization of NaMMT with PMMA

SMBS (0.0072 g) and of DBS (0.0145 g) were dissolved in deionized water (97.0 mL). Nanoclay (5 g) was added

slowly to the mixture under high speed magnetic stirring. MMA (3.0 g) was added to form an emulsion and the mixture purged with dry $N_2$. After mixing for 30 min, AMPS (0.030 g) dissolved in deionised water (10 mL) was added and the mixture heated at 60 °C under $N_2$ for 4 h. The mixture was cooled to room temperature, and the product isolated by filtration. The product was purified by solvent extraction with tetrahydrofuran to remove ungrafted PMMA homopolymer and oven dried at 60 °C for 6 h.

### Characterisation

Functional groups for NaMMT and PMMA-grafted MMT were determined using FTIR (PerkinElmer System 2000). About 2.0 mg of sample was properly mixed with 200 mg of KBr and then ground thoroughly using mortar and pestle. An appropriate amount of the ground sample was pelletized using a SPECAC bolt and nut pelletizer to give a transparent pellet. Each sample was analysed against an air background at 24 scans in the wavenumber range 4000–370 $cm^{-1}$ with a resolution of 4 $cm^{-1}$. Thermal stability and decomposition characteristics were determined using thermogravimetric analyser (PerkinElmer, TGA7) fitted with a thermal analysis controller (TAC7/DX) under $N_2$. The samples were heated from 25 to 900 °C at a heating rate of 15 °C/min. X-ray diffraction analysis was carried out in locked couple mode with a Bruker AXS D8 Advance diffractometer (Cu Kα radiation with $\lambda = 1.5406$ Å, 40 kV, 40 mA, equipped with a PSD Lynx-Eye Si-strip detector (with 196 channels), at room temperature. SEM micrographs were obtained using a scanning electron microscope (Tescan, Vega3, Czech Republic). BET surface area ($S_{BET}$), pore width and pore volume were measured using an automated $N_2$ adsorption analyser (TriStar 3000 V6.08 A, Micromeritics, Norcross, USA).

### Sorption studies

Sorption properties of NaMMT and PMMAgMMT were studied using batch experiments. Synthetic solutions containing a mixture of $Cd^{2+}$ and $Pb^{2+}$ with concentrations of each metal ion ranging from 10 to 50 ppm were prepared from $Cd(NO_3)_2.4H_2O$ and $Pb(NO_3)_2$, respectively, based on earlier work by Chen et al. (2010). The adsorption experiments were carried out to generate isotherm and kinetics data. The conditions used to generate adsorption isotherms were as follows: adsorbent dosage was 1.25 g adsorbent per litre of solution; metal ion concentration ranges were 10–50 ppm for both $Cd^{2+}$ and $Pb^{2+}$; the pH was 5.0 and a temperature of 25 °C for all the adsorption experiments; the shaking time was 6 h. Aliquots were taken after 6 h for measurement with AAS (Thermo Scientific iCE 3000 Series). A blank of distilled water showed no $Cd^{2+}$ or $Pb^{2+}$ contamination. All measurements were performed in triplicate, and mean values calculated and reported. To assess the rate of the adsorption for both $Cd^{2+}$ and $Pb^{2+}$, experiments were carried out under the following conditions: amount of adsorbent used was 1.25 g per 1.0 L of solution; the initial metal concentration for both $Cd^{2+}$ and $Pb^{2+}$ was 50 ppm; the pH was 5.0 and the shaking time was 6 h. Aliquots of sample solutions were withdrawn at set time intervals and the concentration of each heavy metal determined by AAS. The adsorption kinetic studies were carried out separately for each heavy metal ion, and as a mixture.

### Regeneration of spent sorbent

Regeneration of the adsorbents was carried out with 0.1 M $HNO_3$ (80 mL) and the adsorbent was washed with a small volume of 0.01 M NaOH solution until the pH of the filtrate was about 5.0.

## Results and discussion

### Fourier transform infrared (FTIR) spectroscopy

The FTIR spectrum for NaMMT showed stretching vibrations at 467, 527, 801, 843, 886, 919, 1045, 1639, 2927, 3436 and 3636 $cm^{-1}$ (Fig. 1a. These frequencies were attributed to Si–O–Si bending, Si–O–Al bending, O–Si–O asymmetric stretching, Al–OH–Mg deformation, Al–OH–Fe deformation, OH bending ($Al_2OH$), Si–O stretching, H–O–H deformation (interlayer $H_2O$), $–CH_3$ asymmetric stretching, H–O–H stretching (adsorbed $H_2O$) and structural O–H stretching vibrations, respectively (Yuan et al. 2006; Qin et al. 2015; Tran et al. 2015). The FTIR spectrum for PMMA showed peaks at 1453, 1733, 2927 and 2955 $cm^{-1}$ which were attributed to: $–O–CH_3$ (deformation), C=O, $–CH_2$ and $–CH_3$ stretching vibrations, respectively. The presence of the stretching vibrations at 1733 $cm^{-1}$ (C=O) and 1453 $cm^{-1}$ ($–O–CH_3$ asymmetric deformation) in the THF extracted product (PMMAgMMT) confirmed that methyl methacrylate groups were covalently attached to MMT during the grafting process (Rajendran and Mahendran, 2001).

### X-ray diffraction

The characteristic basal reflection peak of NaMMT occurred at $2\theta = 6.22°$ with a basal spacing of 14.2 Å, while that for PMMAgMMT occurred at $2\theta = 5.88°$ with a basal spacing of 15.0 Å (Fig. 1b. An increase in the basal spacing was observed after modification with PMMA. This suggested that PMMA was partially

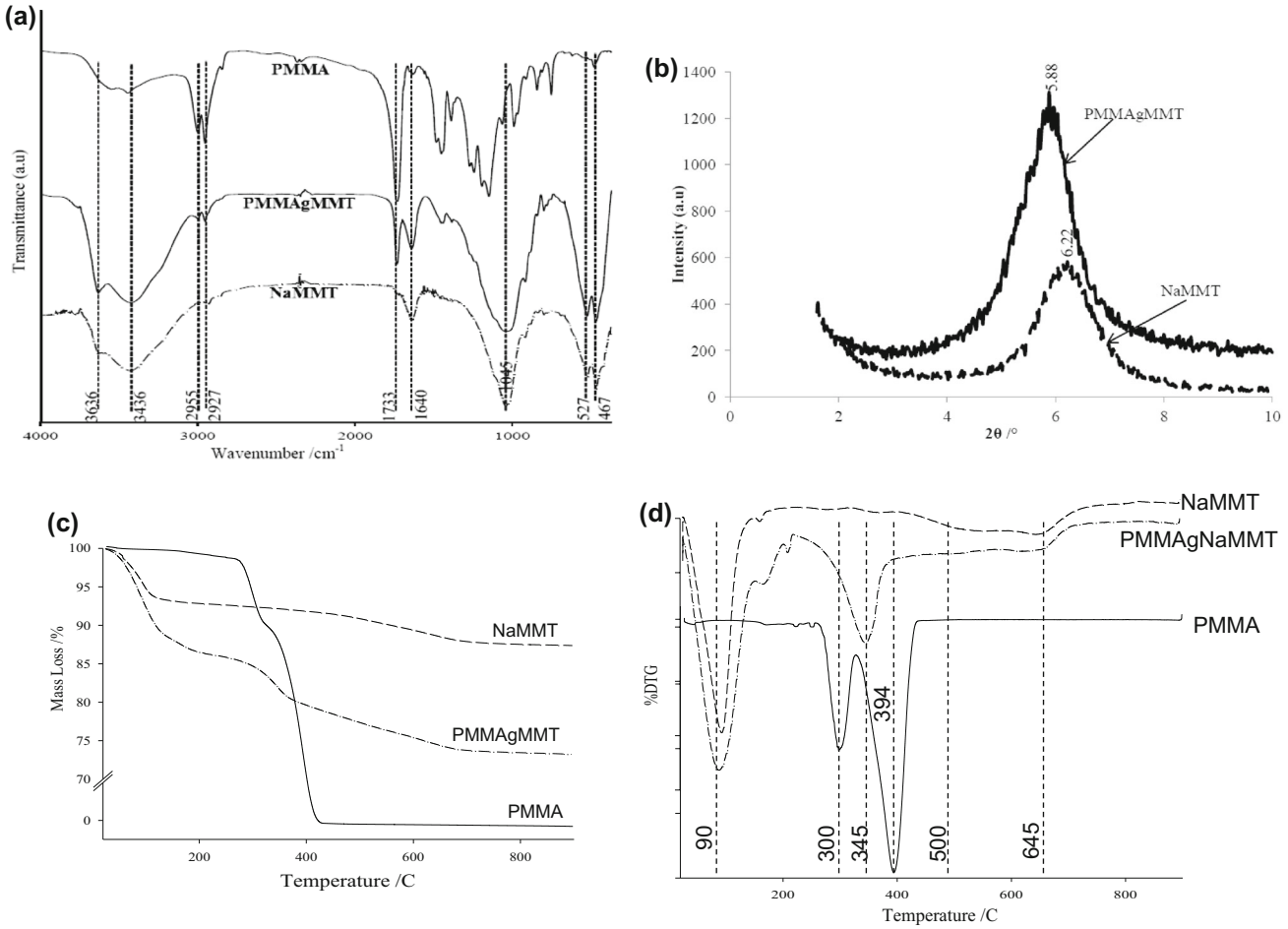


**Fig. 1** **a** FTIR spectra for PMMA, NaMMT and PMMAgMMT, **b** XRD diffractograms for NaMMT and PMMAgMMT, **c** TGA thermograms for PMMA, NaMMT and PMMAgMMT, and **d** Differential thermograms for PMMA, NaMMT and PMMAgMMT

intercalated and polymerized within the interlayer space of the NaMMT, possibly because of the large molecular size of PMMA (Zehhaf et al. 2013; Qin et al. 2015; Tran et al. 2015).

## Thermogravimetric analysis

The thermogram for PMMA showed that its decomposition started from 250 °C up to about 420 °C (Fig. 1c. The PMMA differential thermogram showed two decomposition peaks at 300 and 394 °C. Above 430 °C, all the PMMA was completely decomposed. The thermogram for NaMMT showed a two-step degradation process, at 90 °C, due to loss of adsorbed water, and at 500 °C due to dehydroxylation of the clay structure (Binithat and Sugunan 2006; Qin et al. 2015). The peak at 345 °C in the differential thermogram for PMMAgMMT (Fig. 1d was ascribed to the decomposition of grafted PMMA since the NaMMT differential thermogram did not show a similar peak. The grafting efficiency was estimated from the mass loss at the temperature of 345 °C. This indicated PMMAgMMT contained about 9.0 % by mass of PMMA.

## SEM and BET

Although both micrographs show irregular surfaces and undulations, the morphology of NaMMT had a relatively smooth surface, whereas the PMMAgMMT had a rough surface indicative of the attached PMMA particles (Fig. 2). Similar results were reported for dimercaprol grafted MMT (Tran et al. 2015).

The $S_{BET}$ for NaMMT was about four times higher than that of PMMAgMMT (Table 1). The decrease in surface area is consistent with previous work by Qin et al. (2015) who reported a nine-fold decrease in surface area after intercalating MMT with $Fe^{2+}$ ions and attributed the decrease to the adsorbed $Fe^{2+}$ ions in the montmorillonite layers. The decrease in $S_{BET}$ for PMMAgMMT can thus be ascribed to the occupation of interlayer spaces by PMMA following intercalation, and the relatively smaller decrease

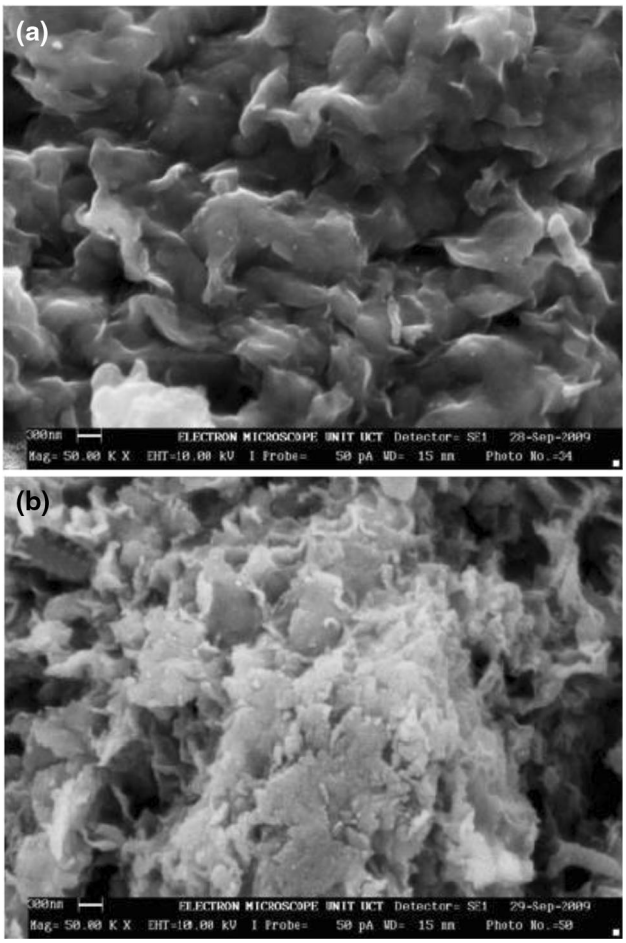


**Fig. 2** SEM micrographs for **a** NaMMT and **b** PMMAgMMT at 50,000× magnification

**Table 1** Porous structural data for NaMMT and PMMAgMMT

| Sorbent | $S_{BET}$ ($m^2/g$) | Pore width (nm) |
|---|---|---|
| NaMMT | 81.6189 | 4.1683 |
| PMMAgMMT | 19.6834 | 8.8875 |

*SBET* specific surface area using BET

could be due to the partial rather than complete intercalation process.

## Adsorption isotherms

The isotherms for $Cd^{2+}$ adsorption onto both NaMMT and PMMAgMMT (Fig. 3a were classified as Langmuir type 2 ($L_2$). The isotherm for $Pb^{2+}$ adsorption onto PMMAgMMT was categorized as Langmuir type 4 ($L_4$), while the isotherm for $Pb^{2+}$ adsorption onto NaMMT was identified as Langmuir type mx ($L_{mx}$) (Hinz 2001). Adsorption isotherms are classified into four major classes based on the slope of the initial portion of the curve of the equilibrium adsorbed amount ($Q_e$) versus equilibrium adsorbate concentration ($C_e$) and thereafter into subgroups (Hinz 2001). This was one of the methods used in the analysis of adsorption data in this study. $Pb^{2+}$ had a higher equilibrium adsorbed amount ($Q_e$) onto both NaMMT and PMMAgMMT for the binary mixture than $Cd^{2+}$. The maximum sorption capacities for NaMMT and PMMAgMMT were 18.73 and 19.27 mg/g for $Cd^{2+}$, and 30.03 and 34.25 mg/g for $Pb^{2+}$, respectively. Other researchers have reported a maximum adsorption capacity of 10.2 mg/g for $Cu^{2+}$ on surfactant treated MMT (Fan et al. 2014), and Xing et al. (2015) reported 99.5 mg/g maximum adsorption of $Pb^{2+}$ on MMT. Similar findings were reported by Lv et al. (2005) in competitive studies of $Cd^{2+}$, $Cu^{2+}$ and $Pb^{2+}$ onto microporous titanosilicate. $Pb^{2+}$ has been reported to inhibit the sorption of $Cd^{2+}$ in biochars, an effect attributed to the differences in ionic radii of the two metals (Wang et al. 2011; Yu et al. 2013). Nonetheless, in the current study, the presence of both heavy metals in solution did not significantly affect their sorption process, as indicated by the isotherm mode, from solution. The experimental data were fitted to linear Langmuir and Freundlich isotherm equations (Eqs. 2 and 3, respectively). $R^2$ values obtained for these models for the two adsorbents ranged between 0.9161 and 0.9984. A slight increase was observed in the uptake of both $Cd^{2+}$ and $Pb^{2+}$ onto PMMAgMMT. The Langmuir model gave higher correlation coefficients ($R^2$) than the Freundlich model (Fig. 3b). The adsorption of $Fe^{2+}$ onto pristine montmorillonite was reported to follow the Langmuir model (Qin et al. 2015), although other studies have reported $Cu^{2+}$ adsorption onto surfactant modified montmorillonite to follow the Freundlich isotherm (Fan et al. 2014). From the Langmuir adsorption capacities, it was observed that slightly less $Cd^{2+}$ was adsorbed onto PMMAgMMT than on NaMMT. This is contrary to what was observed for the adsorption of $Cd^{2+}$ alone onto the same adsorbents, which gave a slightly higher adsorbed amount of $Cd^{2+}$ for PMMAgMMT than NaMMT. For $Pb^{2+}$ adsorption, the trend was maintained as was observed for the adsorption of $Pb^{2+}$ alone (Table 2).

The close correlation between $Q_e$ (Pseudo-second-order) and $Q_0$ (Langmuir) values showed that both models can be used to calculate the maximum amount sorbed for each metal ion.

The amount of each heavy metal sorbed on both NaMMT and PMMAgMMT decreased when the two metals coexisted in solution. A similar trend was observed from the kinetics data. Applying the student's $t$ test ($P = 0.05$) to the data showed that the uptake of $Pb^{2+}$ was significantly reduced by the presence of $Cd^{2+}$ ions in the same solution. Though there was a decrease in $Cd^{2+}$ adsorption in the presence of $Pb^{2+}$, the change was not

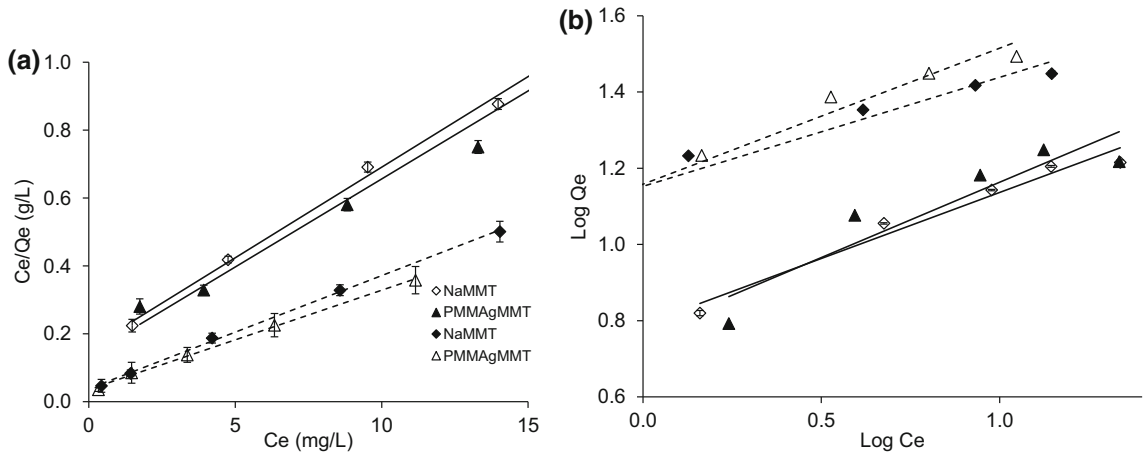


**Fig. 3** **a** Langmuir and **b** Freundlich adsorption isotherms for the adsorption of $Cd^{2+}$ and (*bold lines*) $Pb^{2+}$ (*dashed lines*) on NaMMT and PMMAgMMT

**Table 2** Best-fit parameters for isotherm and kinetic models for the adsorption of (a) $Cd^{2+}$ and (b) $Pb^{2+}$ on NaMMT and PMMAgMMT

| Model | Parameter 1 | Parameter 2 | $R^2$ |
|---|---|---|---|
| a. $Cd^{2+}$ | | | |
| NaMMT | | | |
| Langmuir | $b = 0.3408$ | $Q = 15.70$ mg $g^{-1}$ | 0.9736 |
| Freundlich | $K = 5.01$ mg $g^{-1}$ | $n = 3.16$ | 0.9613 |
| First order | $k_1 = 1.40 \times 10^{-2}$ L $min^{-1}$ | $Q_e = 7.18$ mg $g^{-1}$ | 0.9908 |
| Second order | $k_2 = 4.60 \times 10^{-3}$ g $mg^{-1}$ $min^{-1}$ | $Q_e = 14.81$ mg $g^{-1}$ | 0.9991 |
| PMMAgMMT | | | |
| Langmuir | $b = 0.3772$ | $Q = 14.97$ mg $g^{-1}$ | 0.9927 |
| Freundlich | $K = 4.09$ mg $g^{-1}$ | $n = 2.41$ | 0.9237 |
| First order | $k_1 = 1.96 \times 10^{-2}$ L $min^{-1}$ | $Q_e = 3.34$ mg $g^{-1}$ | 0.9847 |
| Second order | $k_2 = 2.84 \times 10^{-2}$ g $mg^{-1}$ $min^{-1}$ | $Q_e = 12.30$ mg $g^{-1}$ | 0.9988 |
| b. $Pb^{2+}$ | | | |
| NaMMT | | | |
| Langmuir | $b = 0.8627$ | $Q = 22.67$ mg $g^{-1}$ | 0.9950 |
| Freundlich | $K = 9.32$ mg $g^{-1}$ | $n = 3.51$ | 0.9658 |
| First order | $k_1 = 9.21 \times 10^{-3}$ L $min^{-1}$ | $Q_e = 6.24$ mg $g^{-1}$ | 0.9608 |
| Second order | $k_2 = 5.36 \times 10^{-3}$ g $mg^{-1}$ $min^{-1}$ | $Q_e = 21.37$ mg $g^{-1}$ | 0.9998 |
| PMMAgMMT | | | |
| Langmuir | $b = 0.8022$ | $Q = 24.39$ mg $g^{-1}$ | 0.9984 |
| Freundlich | $K = 11.30$ mg $g^{-1}$ | $n = 3.08$ | 0.9161 |
| First order | $k_1 = 1.47 \times 10^{-2}$ L $min^{-1}$ | $Q_e = 6.24$ mg $g^{-1}$ | 0.9796 |
| Second order | $k_2 = 6.61 \times 10^{-3}$ g $mg^{-1}$ $min^{-1}$ | $Q_e = 22.52$ mg $g^{-1}$ | 0.9997 |

statistically significant at 95 % confidence level. The reduction observed was attributed to the competition between the metals ions for the same adsorption sites on the adsorbent surface (Chen et al. 2010). However, the adsorption capacities found for each heavy metal were still significantly high, thus making the adsorbents suitable for use in the treatment of heavy metals contaminated water.

The uptake of $Cd^{2+}$ was consistently lower compared with $Pb^{2+}$ uptake regardless of the adsorbent. The student's *t*-test showed that the uptake of $Cd^{2+}$ was statistically different from $Pb^{2+}$ uptake at 95 % confidence level. Mobasherpour et al. (2012) reported a similar trend for the adsorption of $Cd^{2+}$ and $Pb^{2+}$ on nano-crystallite hydroxyapatite from aqueous solution. The higher affinity of $Pb^{2+}$ for the adsorbent was attributed to the smaller hydrated radius of $Pb^{2+}$ (4.01 Å) and its low hydration energy ($Pb^{2+} = -1481$ kJ/mol) relative to $Cd^{2+}$ (4.19 Å, −2106 kJ/mol). Chen et al. (2010) studied the adsorption

of $Cd^{2+}$, $Cu^{2+}$ and $Pb^{2+}$ onto nano-hydroxyapatite and observed similar behaviour. Pavasant et al. (2006) also observed the same trend for $Zn^{2+}$, $Cu^{2+}$, $Cd^{2+}$ and $Pb^{2+}$ adsorption onto marine green macroalgae.

### Adsorption kinetics

The systems reached equilibrium within 3 h and the uptake of $Pb^{2+}$ was higher than the uptake of $Cd^{2+}$ to both sorbents (Fig. 4). From the kinetic data (Table 2), it was observed that the pseudo second-order model had higher $R^2$ values than the pseudo first-order model. The adsorption of $Cd^{2+}$ remained the same for the two adsorbents while $Pb^{2+}$ uptake increased slightly for PMMAgMMT. The uptake of $Pb^{2+}$ was higher than that of $Cd^{2+}$ for both adsorbents. Chen et al. (2010) obtained similar results for the aqueous adsorption of $Cd^{2+}$, $Pb^{2+}$ and $Cu^{2+}$ with nano-hydroxyapatite. The differences in the affinities of the metals for the adsorbents could still be attributed to their respective ionic radii. The pseudo first-order and pseudo second-order plots for $Cd^{2+}$/$Pb^{2+}$ adsorption from binary solutions (Fig. 4a, b show that the pseudo second-order model had the highest $R^2$ values for both metal ions (Table 2). However, the pseudo first-order $R^2$ values were also relatively high (>0.9600) suggesting that the data could be adequately described by both models. The reason for a lower $Q_e$ value for $Cd^{2+}$ adsorption onto PMMAgMMT than NaMMT was not clear. Antoniadis et al. (2007) reported a similar trend in the adsorption of Cd, Ni and Zn onto sewage sludge-amended soil.

### Regeneration of spent adsorbent

As expected, the amount of both $Cd^{2+}$ and $Pb^{2+}$ adsorbed decreased with an increase in the number of regeneration cycles (Fig. 5a). $Pb^{2+}$ uptake decreased by about 27 % while $Cd^{2+}$ uptake decreased by about 23 % after three regeneration cycles. The slight decrease in the uptake of the two heavy metals suggested that PMMAgMMT can be used repeatedly for at least three regeneration cycles without a significant loss in the adsorption capacity. The desorption experiments for $Pb^{2+}$ from PMMAgMMT showed that up to 96 % of the adsorbed amount could be desorbed by using 80 mL of 0.1 M $HNO_3$, while 100 % of $Cd^{2+}$ could be desorbed under similar conditions, the differences being attributed to higher affinity of $Pb^{2+}$ for the adsorbent. FTIR spectra of the regenerated sorbent showed a peak at 420 $cm^{-1}$ for PMMAgMMT at zero and two regeneration cycles, confirming the existence of a metal–oxygen bond (Fig. 5b) (de Portilla 1974). Chemisorption is thus a likely mechanism for the removal of $Cd^{2+}$ and $Pb^{2+}$ from aqueous solution.

## Conclusion

The grafting of PMMA by emulsion copolymerization onto NaMMT was confirmed by FTIR, TGA and XRD results. Analysis of the materials showed that PMMA was successfully bonded onto the silanol groups on the montmorillonite clay. Adsorption studies for $Cd^{2+}$ and $Pb^{2+}$ adsorption on NaMMT and PMMAgMMT separately and as binary solutions, have demonstrated that it is possible to improve the sorption properties of montmorillonite clay by grafting the nanoclay with organic polymers like poly (methyl methacrylate). $Pb^{2+}$ had a significantly higher sorption affinity for both NaMMT and PMMAgMMT compared with $Cd^{2+}$. Competitive adsorption results showed a decrease in the uptake of both heavy metals. The competitive sorption of $Cd^{2+}$ and $Pb^{2+}$ did not significantly affect the sorption process of each and the mechanism of adsorption. The data also obeyed the Langmuir model and

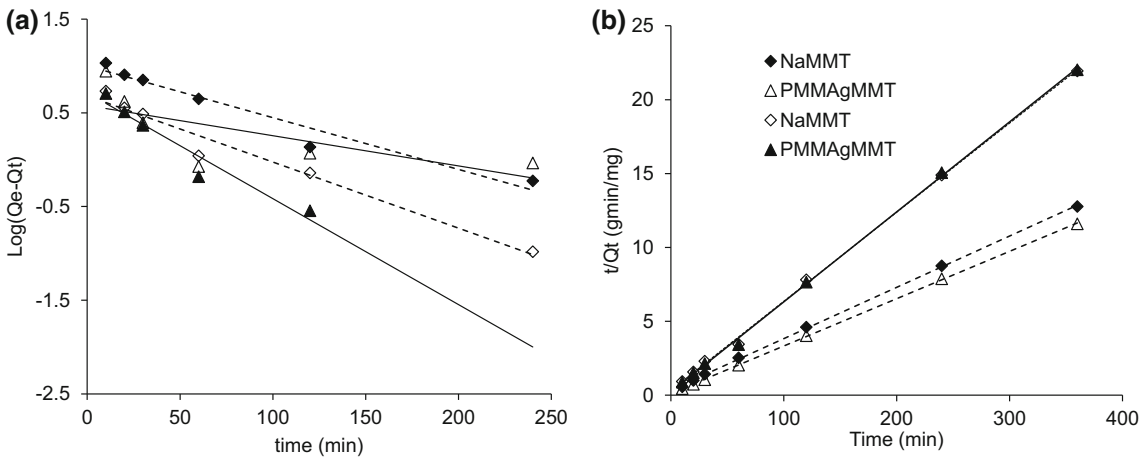


**Fig. 4** **a** Pseudo-first order and **b** pseudo-second order kinetic plots for the adsorption of $Cd^{2+}$ and $Pb^{2+}$ on NaMMT and PMMAgMMT

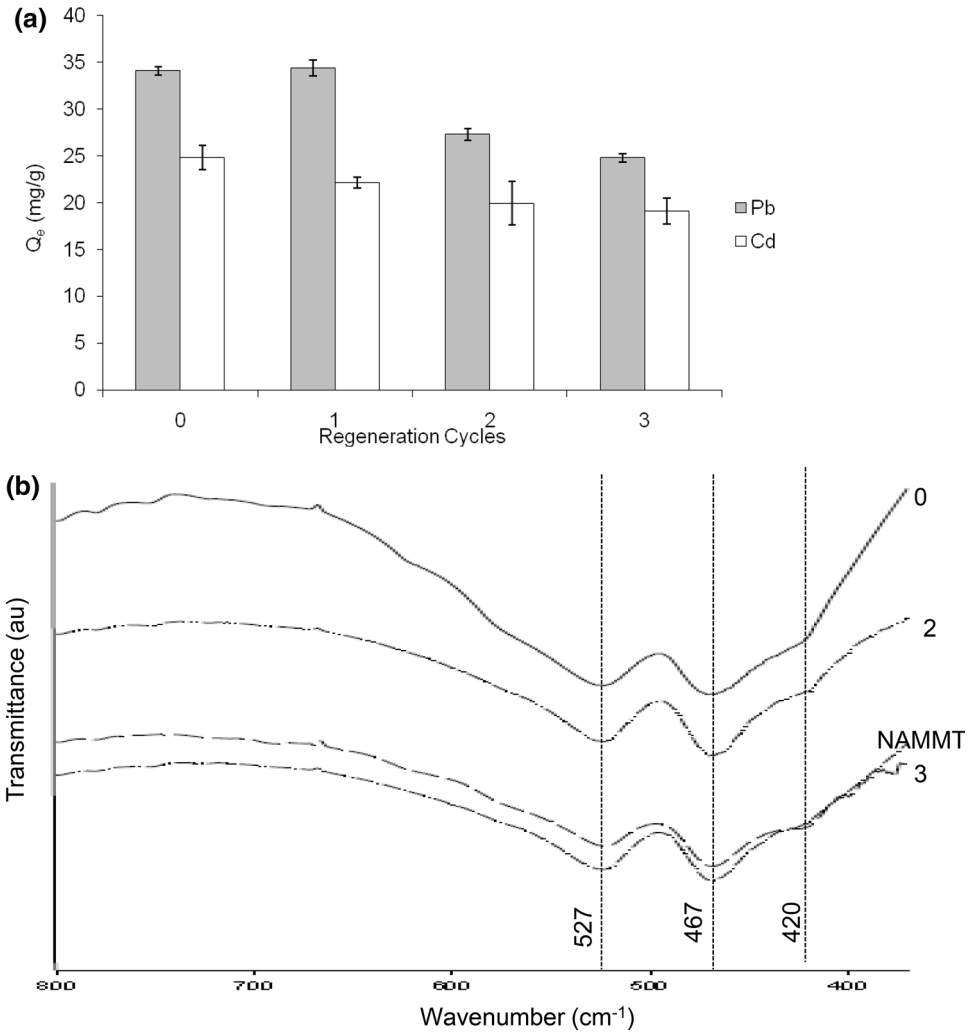


**Fig. 5** **a** Regeneration behaviour of PMMAgMMT after the adsorption of $Cd^{2+}$ and $Pb^{2+}$, and **b** FTIR spectra for PMMAgMMT after regeneration

pseudo second-order model. Although there was a decrease in both $Cd^{2+}$ and $Pb^{2+}$ uptake, the adsorbed amounts of each metal still remained relatively high, thus making the sorbents suitable for the simultaneous removal of $Cd^{2+}$ and $Pb^{2+}$ from contaminated water. The fact that PMMAgMMT could be regenerated and reused for three cycles without a significant loss in sorption capacity allows for the development of a cost-effective sorbent. Overall, if properly developed through the grafting of suitable organic groups, montmorillonite nanoclay can result in low-cost, efficient and effective nanotechnology based water treatment systems.

**Acknowledgments** The authors would like to thank Govan Mbeki Research and Development Centre (University of Fort Hare) and iThemba Labs for access to XRD instruments.



## References

Alfven T, Jarup L, Elinder CG (2002) Cadmium and lead in blood in relation to low bone mineral density and tubular proteinuria. Environ. Health Persp. 110:699–702

Antoniadis V, Tsadilas CD, Ashworth DJ (2007) Monometal and competitive adsorption of heavy metals by sewage sludge-amended soil. Chemosphere 68:489–494

Arief VO, Trilestari K, Sunarso J, Indraswati N, Ismadji S (2008) Recent progress on biosorption of heavy metals from liquids using low cost biosorbents: characterization, biosorption parameters and mechanism studies. Clean Soil Air Water 36:937–962

Binithat NN, Sugunan S (2006) Preparation and characterisation and catalytic activity of titania-pillared montmorillonite clays. Micropor. Mesopor. Mater. 93:82–89

Cabrera A, Cox L, Spokas K, Hermosin MC, Cornejo J, Koskinen WC (2014) Influence of biochar amendments on the sorption-

desorption of aminocyclopyrachlor, bentazone and pyraclostrobin pesticides to agricultural soil. Sci Total Environ 470–471:438–443

Cao F, Bai P, Li H, Ma Y, Deng X, Zhao C (2009) Preparation of polyethersulfone-organophilic montmorillonite hybrid particles for the removal of bisphenol A. J Hazard Mater 162:791–798

Chen SB, Ma YB, Chen L, Xian K (2010) Adsorption of aqueous $Cd^{2+}$, $Pb^{2+}$, $Cu^{2+}$ ions by nano-hydroxyapatite: single- and multi-metal competitive study. Geochem J 44:233–239

De Portilla VIS (1974) Infrared spectroscopic investigation of the structure of some natural arsenates and the nature of H-bonds in their structures. Can Mineral 12:262–268

Delval F, Crini G, Morinc N, Vebrel J, Bertini S, Torri G (2002) The sorption of several types of dye on crosslinked polysaccharides derivatives. Dyes Pigm 53:79–92

Fan H, Zhou L, Jiang X, Huang Q, Lang W (2014) Adsorption of $Cu^{2+}$ and methylene blue on dodecyl sulfobetaine surfactant-modified montmorillonite. Appl Clay Sci 95:150–158

Garg VK, Kumar R, Gupta R (2004) Removal of malachite green dye from aqueous solution by adsorption using agro-industry waste: a case study of prosopis cineraria. Dyes Pigm 62:1–10

Gwenzi W, Musarurwa T, Nyamugafata P, Chaukura N, Chaparadza A, Mbera S (2014) Adsorption of $Zn^{2+}$ and $Ni^{2+}$ in a binary aqueous solution by biosorbents derived from sawdust and water hyacinth (*Eichhornia crassipes*). Water Sci Technol 70:1419–1427

Hinz C (2001) Description of sorption data with isotherm equations. Geoderma 99:225–243

Jarup L, Hellstrom L, Alfven T, Carlsson MD, Grubb A, Persson B, Pettersson C, Spang G, Schutz A, Elinder CG (2000) Low level exposure to cadmium and early kidney damage: the OSCAR study. Occup Environ Med 57:668–672

Jin T, Nordberg G, Ye T, Bo M, Wang H, Zhu G, Kong Q, Bernard A (2004) Osteoporosis and renal dysfunction in a general population exposed to cadmium in China. Environ Res 96:353–359

Kazantzis G (2004) Cadmium, osteoporosis and calcium metabolism. Biometals 17:493–498

Kobya M, Demirbas E, Senturk E, Ince M (2005) Adsorption of heavy metal ions from aqueous solutions by activated carbon prepared from apricot stone. Bioresour Technol. 96:1518–1521

Kumar D, Singh A, Gaur JP (2008) Mono-component versus binary isotherm models for Cu (II) and Pb(II) sorption from binary metal solution by the green alga pithophora oedogonia. Bioresour Technol. 99:8280–8287

Lv L, Hor MP, Su F, Zhao XS (2005) Competitive adsorption of $Pb^{2+}$, $Cu^{2+}$ and $Cd^{2+}$ ions on microporous titanosilicate ETS-10. J Colloid Interface Sci 287:178–184

Mobasherpour I, Salahi E, Pazouki M (2012) Comparative of the removal of $Pb^{2+}$, $Cd^{2+}$ and $Ni^{2+}$ by nano crystallite hydroxyapatite from aqueous solutions: adsorption isotherm study. Arab J. Chem. 5:439–446

Nawrot TS, Staessen JA, Roels HA, Munters E, Cuypers A, Richart T, Ruttens A, Smeets K, Clijsters H, Vangronsveld J (2010) Cadmium exposure in the population: from health risks to strategies of prevention. Biometals 23:769–782

Pavasant P, Apiratikul R, Sungkhum V, Suthiparinyanont P, Wattanachira S, Marhaba TF (2006) Biosorption of $Cu^{2+}$, $Cd^{2+}$, $Pb^{2+}$, and $Zn^{2+}$ using dried marine green macroalga *Caulerpa lentillifera*. Bioresour Technol 97:2321–2329

Qin D, Niu X, Qiao M, Liu G, Li H, Meng Z (2015) Adsorption of ferrous ions onto montmorillonites. Appl Surf Sci 333:170–177

Rajendran SKR, Mahendran O (2001) An electrochemical investigation on PMMA/PVDF blend-based polymer electrolytes. Mater Lett 49:172–179

Rebitanim NZ, Ghani WA, Mahmoud DK, Rebitanin NA, Salleh MAM (2012) Adsorption of methylene blue by agricultural solid waste pyrolysed from EFB biochar. J. Purity Util. React. Environ. 1:346–360

Ruziwa DT, Chaukura N, Gwenzi W, Pumure I (2015) Removal of $Zn^{2+}$ and $Pb^{2+}$ from water using sulphonated waste polystyrene. J Environ Chem Eng 3:2528–2537

Teemu H (2007) Removal of cadmium, lead and arsenic from water by lactic acid bacteria. Functional Foods Forum, Turkey

Tran L, Wu P, Zhu Y, Liu S, Zhu N (2015) Comparative study of Hg(II) adsorption by thiol- and hydroxyl-containing bifunctional montmorillonite and vermiculite. Appl Surf Sci 256:91–101

Wang S, Dong Y, He M, Chen L, Yu X (2009) Characterization of GMZ bentonite and its application in the adsorption of Pb(II) from aqueous solutions. Appl Clay Sci 43:164–171

Wang XS, Miao HH, He W, Shen HL (2011) Competitive adsorption of Pb(II), Cu(II), and Cd(II) ions on wheat-residue derived black carbon. J Chem Eng Data 56:444–449

Xing X, Lv G, Zhu W, He C, Liao L, Mei L, Li Z, Li G (2015) The binding energy between the interlayer cations and montmorillonite layers and its influence on $Pb^{2+}$ adsorption. Appl Clay Sci 112–113:117–122

Yu J, Wang L, Chi R, Zhang Y, Xu Z, Guo J (2013) Competitive adsorption of $Pb^{2+}$ and $Cd^{2+}$ on magnetic modified sugarcane bagasse prepared by two simple steps. Appl Surf Sci 268:163–170

Yuan P, He H, Bergaya FA, Wu D, Zhou Q, Zhu J (2006) Synthesis and characterization of delaminated iron-pillared clay with meso-microporous structure. Microporous Mesoporous Mater 88:8–15

Zehhaf A, Morallon E, Benyoucef A (2013) Polyaniline/montmorillonite nanocomposites obtained by in situ intercalation and oxidative polymerization in cationic modified-clay (sodium, copper and iron). J Inorg Organomet Polym 23:1485–1491

Zhu R, Zhu R, Ge F, Xu Y, Liu J, Zhu J, He H (2016a) Effect of heating temperature on the sequestration of $Cr^{3+}$ cations on montmorillonite. Appl Clay Sci 121–122:111–118

Zhu R, Chen Q, Zhou Q, Xi Y, Zhu J, He H (2016b) Adsorbents based on montmorillonite for contaminant removal from water: a review. Appl Clay Sci 123:239–258